Water Vapour and Methane Coupling in the Stratosphere observed with SCIAMACHY Solar Occultation Measurements

Stefan Noël, Katja Weigel, Klaus Bramstedt, Alexei Rozanov, Mark Weber, Heinrich Bovensmann, and John P. Burrows

Institute of Environmental Physics, University of Bremen, FB 1, P.O. Box 330440, 28334 Bremen, Germany

Correspondence to: S. Noël (stefan.noel@iup.physik.uni-bremen.de)

Abstract.

An improved stratospheric water vapour data set has been derived from SCIAMACHY/ENVISAT solar occultation measurements. It is based on the same algorithm which has already been successfully applied to methane and carbon dioxide retrievals, thus resulting in a consistent data set for theses three constituents covering the altitudes 17–45 km, the latitude range between
5 about 50 and 70°N, and the time interval August 2002 to April 2012.

The new water vapour data agree with collocated results from ACE-FTS and MLS/Aura within about 5%. A significant positive water vapour trend for the time 2003–2011 is observed at lower stratospheric altitudes of about 0.015 ppmv year^{-1} around 17 km. Between 30 and 37 km the trends become significantly negative (about -0.01 ppmv year^{-1}).

The combined analysis of the SCIAMACHY methane and water vapour time series reveals that stratospheric methane and
10 water vapour are strongly correlated and show a clear temporal variation related to the Quasi-Biannual-Oscillation (QBO). Above about 20 km most of the water vapour seems to be produced by methane, but short-term fluctuations and a temporal variation on a scale of 5–6 years are observed.

At lower altitudes the balance between water vapour and methane is affected by stratospheric transport of water vapour and methane from the tropics to higher latitudes via the shallow branch of the Brewer-Dobson circulation and by the increasing
15 methane input into the stratosphere due to the rise of tropospheric methane after 2007.

1 Introduction

Water vapour (H_2O) and methane (CH_4) are beside carbon dioxide (CO_2) the most important greenhouse gases and therefore determine the climate on our planet. In the stratosphere they also play an important role in chemistry, e.g. in ozone loss due to HO_x gas phase chemistry and heterogeneous reactions on polar stratospheric clouds (PSCs), see e.g. Seinfeld and Pandis
20 (2006). However, since both water vapour and methane (and also carbon dioxide) are very stable, they can also be used as dynamical tracers.

Methane is mainly produced in the troposphere by various natural and anthropogenic processes. The identification of methane sources and sinks by the use of satellite measurements is currently a major topic of scientific investigations (see

e.g. Buchwitz et al., 2017, and references therein). Due to its long lifetime, tropospheric methane is then transported into the stratosphere.

Most of the water vapour is of natural origin and located in the troposphere. It enters the stratosphere mainly through the tropical tropopause layer (TTL; see e.g. Randel et al., 2004, Randel and Jensen, 2013, and references therein). There, the

5 cold temperatures of the tropical tropopause yield a 'cold trap' (see e.g. Read et al., 2004, Holton and Gettelman, 2001) causing lower concentrations of water vapour in the stratosphere than in the troposphere. The water vapour, which enters the stratosphere through the TTL, is then transported via the Brewer-Dobson circulation from the tropics to higher latitudes. The Brewer-Dobson circulation also controls the tropical upwelling and freeze-drying process that in turn determines the stratospheric entry of water vapour in the tropics (Randel et al., 2006; Dhomse et al., 2008).

10 In the middle stratosphere and above, water vapour is in fact mainly produced from oxidation of stratospheric methane via the reaction

$$CH_4 + OH \rightarrow H_2O + CH_3 \tag{R1}$$

Via various photochemical processes (see e.g. le Texier et al., 1988) the CH_3 is converted first to HCHO and then to H_2O resulting in the net reaction:

15 $$CH_4 + 2O_2 \rightarrow 2H_2O + CO_2 \tag{R2}$$

According to this reaction one methane molecule finally produces two water vapour molecules, which means that the sum of volume mixing ratios $[H_2O] + 2[CH_4]$, referred to as potential water (PW), see e.g. Nassar et al. (2005), is expected to be roughly conserved in the stratosphere if no changes in mixing of air masses occur and if variations in H_2 can be neglected. The latter is in fact not always the case, as investigations by e.g. Juckes (2007) and Wrotny et al. (2010) indicate.

20 The combination of water vapour and methane data can therefore give information about sources and sinks of water vapour and dynamical effects in the stratosphere. This requires long-term data sets, which can be provided by satellite measurements; in the best case both water vapour and methane should be measured by the same instrument.

So far, data sets which fulfil these criteria are available only from a few instruments. This includes the Halogen Occultation Experiment (HALOE; Russell et al., 1993) on the Upper Atmospheric Research Satellite (UARS) measuring in solar occul-

25 tation geometry from 1991 until 2005, see Rosenlof (2002). Furthermore, the Atmospheric Chemistry Experiment Fourier Transform Spectrometer (ACE-FTS) on SCISAT (Bernath et al., 2005) is operating also in solar occultation geometry and provides scientific data since 2004. Among the numerous ACE-FTS data products are also methane and water vapour, see e.g. Nassar et al. (2005). Stratospheric methane and water vapour profiles were also measured by the Michelson Interferometer for Passive Atmospheric Sounding (MIPAS; Fischer et al., 2008) on ENVISAT from 2002 to 2012 in limb geometry, see e.g. Payan

30 et al. (2009); Laeng et al. (2015); Plieninger et al. (2016). Some early results from a combination of stratospheric methane and water vapour from MIPAS are given in Payne et al. (2005). Although primarily dedicated to measurements of polar meso- spheric clouds (PMCs), the Aeronomy of Ice in the Mesosphere (AIM) Solar Occultation for Ice Experiment (SOFIE; Gordley et al., 2009) instrument also provides profiles of water vapour and methane. In the context of validation of the SOFIE V1.3

methane product, Rong et al. (2016) presented results from a combination of SOFIE and MIPAS methane with water vapour profiles from the Aura Microwave Limb Sounder (MLS; Waters et al., 2006) on Aura.

The SCanning Imaging Absorption spectroMeter for Atmospheric CHartographY (SCIAMACHY; Bovensmann et al., 1999; Gottwald and Bovensmann, 2011) on ENVISAT performed measurements in various viewing geometries over a large spectral range from the UV to the SWIR. Among these are solar occultation measurements, which cover – depending on season – the spatial region between about 50°N and 70°N. Noël et al. (2016) presented an updated data set for stratospheric methane derived from SCIAMACHY solar occultation using the onion-peeling DOAS (ONPD) method. Already some years ago, Noël et al. (2010) showed first retrieval results for stratospheric water vapour profiles from SCIAMACHY which were based on a similar algorithm. Recently, the improved method used by Noël et al. (2016) has also been applied to water vapour, resulting in a consistent set of SCIAMACHY stratospheric water vapour and methane data.

In this manuscript, we shortly describe the updated water vapour algorithm in section 2. We then present the new water vapour results in section 3, which also includes a first validation by comparison with independent data sets and a combination of the new water vapour data with the methane data from Noël et al. (2016). The results are discussed in section 4. The conclusions are then presented in section 5.

2 H₂O Retrieval

The retrieval method used in this study is essentially the same as described in Noël et al. (2016), therefore only the principle idea is explained here.

We use transmission spectra as function of viewing (tangent) altitude derived from SCIAMACHY solar occultation measurements. For the water vapour retrieval, we take data in the spectral range 928 nm to 968 nm. The ONPD retrieval is then based on a combination of a weighting function DOAS fit (see e.g. Perner and Platt, 1979; Burrows et al., 1999; Coldewey-Egbers et al., 2005) with a classical onion peeling method (see e.g. Russell and Drayson, 1972). The retrieval altitude grid is 0 to 50 km in 1 km steps. The measured spectra are interpolated to this grid. The analysis starts at the top level and then proceeds downwards, taking into account the results from the upper levels. At each level, we determine the water vapour density from the difference between the measured transmission and a modelled one. This is done by fitting to the data a set of factors describing the change of an atmospheric parameter in combination with corresponding weighting functions. Such a weighting function describes the change of the spectrum when changing a certain parameter, e.g. the water vapour concentration at this altitude. In the present case we consider in addition to water vapour also changes in ozone (which also absorbs in the spectral window used). Actual pressure and temperature profiles have been taken from ECMWF ERA Interim data (Dee et al., 2011). The related weighting functions have been determined from radiative transfer calculations using the SCIATRAN model (Rozanov et al., 2014).

To account for spectrally broadband effects resulting from e.g. aerosols we also fit a polynomial to the spectra. A possible misalignment of the wavelength axis of the measured data is considered by fitting corresponding shift and squeeze parameters.

An example for the results of the fitting procedure is shown in Fig. 1. As can be seen, the measured transmissions can be reproduced within an error of about 0.1%.
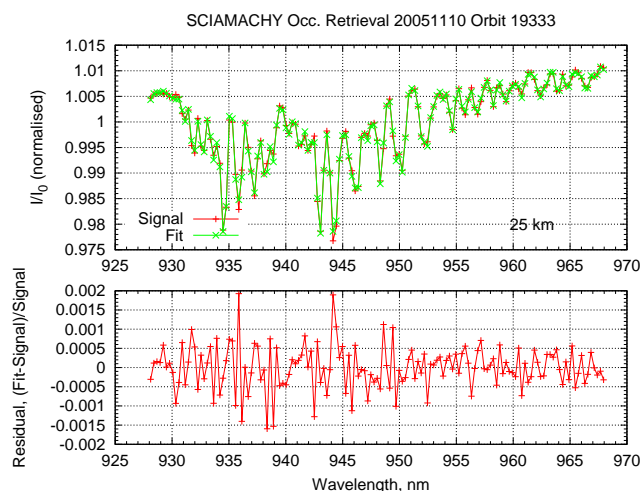
Figure 1. Example of a spectral fit. Top: normalised measured spectrum (red line) and fitted spectrum (green line) at 25 km tangent altitude. Bottom: resulting residual, i.e. relative difference between measurement and fit.

After the retrieval several additional corrections are performed as described in Noël et al. (2016):

- The retrieved profiles are smoothed with a 4.3 km boxcar to account for the vertical resolution of the measurements and to reduce oscillations in the retrieved number densities.

- Additional correction factors are applied for non-linearity and saturation effects (due to the limited spectral resolution of the measurements).

- The resulting errors are multiplied by a factor of 0.66 to correct for correlations between different layers not considered in the fit (see Noël et al., 2016, for details).

The resulting number density profiles are converted to volume mixing ratios (VMRs) using ECMWF pressure and temperature. The useful vertical range of the SCIAMACHY ONPD data is currently considered to be 17 to 45 km, mainly limited by noise and numerical effects at the upper altitudes and by tropospheric effects (e.g. clouds and increased refraction)) at the lower altitudes.

3 Results

3.1 H_2O example data

Fig. 2 shows as an example the resulting water vapour VMR profile from a SCIAMACHY occultation measurement in November 2005. In green the result of the updated retrieval (V4.5.2) is shown. For comparison, the corresponding profile derived with the Noël et al. (2010) algorithm (V2.0.2) is plotted in red, and a collocated ACE-FTS profile (V3.5) in blue. The error bars
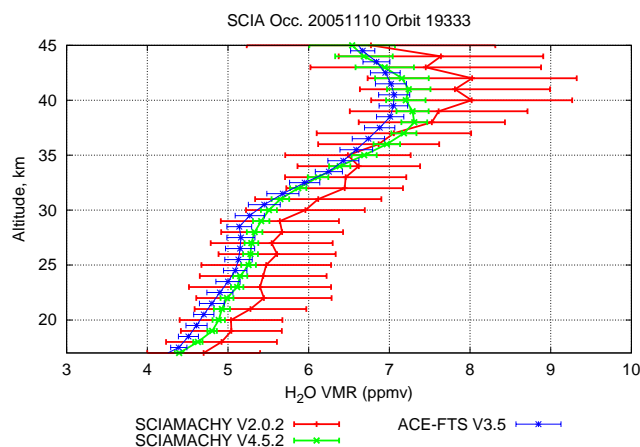
Figure 2. Example for H_2O VMR profiles. Red: previous product (V2.0.2) from Noël et al. (2010). Green: current product (V4.5.2). Blue: collocated profile from ACE-FTS V3.5.

denote the errors given in the products. Obviously, the new SCIAMACHY product is closer to the ACE-FTS results and the reported error is largely reduced compared to the older version. This is due to the improved retrieval method and to the updated calculation of errors as described in Noël et al. (2016).

3.2 H_2O validation

5 A large number of water vapour data products have contributed to the second SPARC (Stratosphere-troposphere Processes And their Role in Climate) water vapour assessment (WAVAS-II; see e.g. Lossow et al., 2017, further publications in preparation). One activity of WAVAS-II was the inter-comparison of the different data sets, including a preliminary earlier version (V4.2.1) of the SCIAMACHY ONPD product. The performance of the V4.2.1 product is very similar to the V4.5.2 product described in this manuscript. We therefore show in this section only two comparisons with collocated ACE-FTS (see e.g. Nassar et al., 2005)

10 and MLS (see e.g. Carr et al., 1995; Lambert et al., 2007) data as an example. In both cases the spatial collocation criterium is 800 km. For ACE-FTS we use only sunset data, meaning that the local time difference to the SCIAMACHY data is usually less than one hour. For MLS we use a maximum time distance of 9 hours to the SCIAMACHY measurements and always take the closest match. This results in 1330 collocations with ACE-FTS and almost 35000 collocations with MLS between 2004 and 2012.

15 Fig. 3 shows the results of the comparison between the SCIAMACHY ONPD V4.5.2 water vapour profiles and ACE-FTS V3.5 data. The MLS results are displayed in Fig. 4. The SCIAMACHY water vapour profiles agree with both data sets within less than 5%. The SCIAMACHY water vapour VMRs are usually slightly higher than those of ACE-FTS, but (except for the lowest altitudes) typically smaller than MLS VMRs. A small vertical oscillation of 1–2% amplitude is visible in the differences; this is caused by the SCIAMACHY data and probably a retrieval artifact which was also seen in the SCIAMACHY ONPD

20 methane and CO_2 data (Noël et al., 2016). The observed deviations are within the typical error of the products.
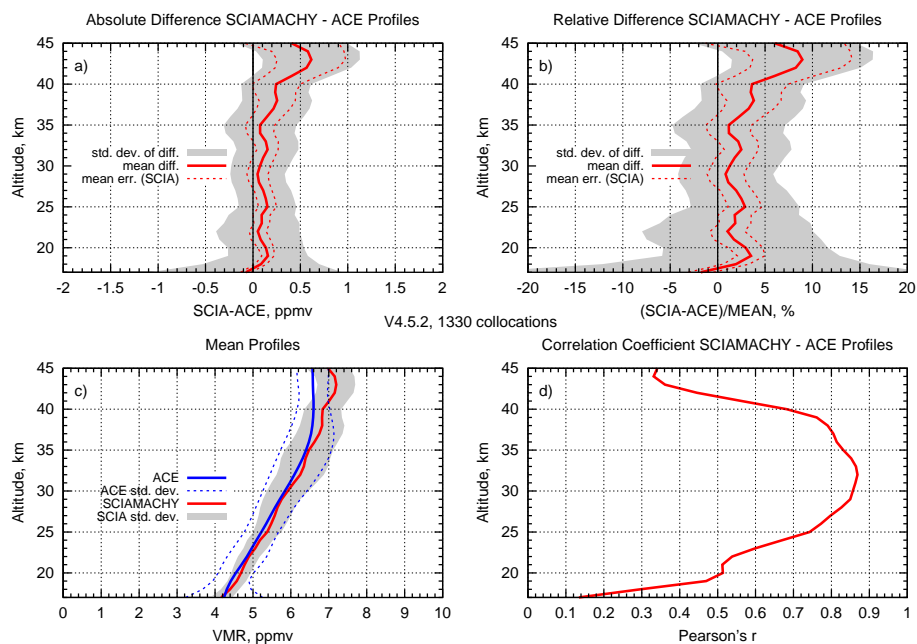
Figure 3. Comparison of retrieved SCIAMACHY H_2O profiles with ACE-FTS data 2004–2012. **(a)** Mean absolute difference plus/minus one standard deviation (shaded area) and mean absolute error of SCIAMACHY data (dotted line). **(b)** Mean relative difference plus/minus one standard deviation (shaded area) and mean relative error of SCIAMACHY data (dotted line). **(c)** Mean profiles and standard deviations (red: SCIAMACHY, blue: ACE-FTS). **(d)** Correlation between SCIAMACHY and ACE-FTS data.

3.3 Time series

The ONPD algorithm for water vapour has been applied to the whole set of SCIAMACHY measurements from August 2002 to April 2012. From the individual VMR profiles daily averages have been computed which are shown in Fig. 5 as function of time and altitude. As can be seen from the top curve in this figure, there is a direct relation between the latitude of the observation and the time in the year. Observations in summer are typically at lower latitudes than in winter. This pattern is caused by the sun-fixed orbit of ENVISAT and thus repeats every year. The average tropopause height, derived from collocated ECMWF data and shown by the black line near the bottom, varies in a similar way. The SCIAMACHY solar occultation data have therefore a specific temporal and spatial sampling.

The SCIAMACHY water vapour profiles perform in general as expected: Highest VMRs (up to about 8 ppmv) occur at upper altitudes, lowest VMRs at lower altitudes. The variation with time follows roughly the tropopause / latitude pattern.

For a more detailed analysis including the combination of water vapour and methane results, we computed monthly anomalies from the SCIAMACHY H_2O data in the same way as described Noël et al. (2016) and put them in relation to the CH_4 data from this study. This is done by first averaging the daily data over the months and then subtracting the long-term average
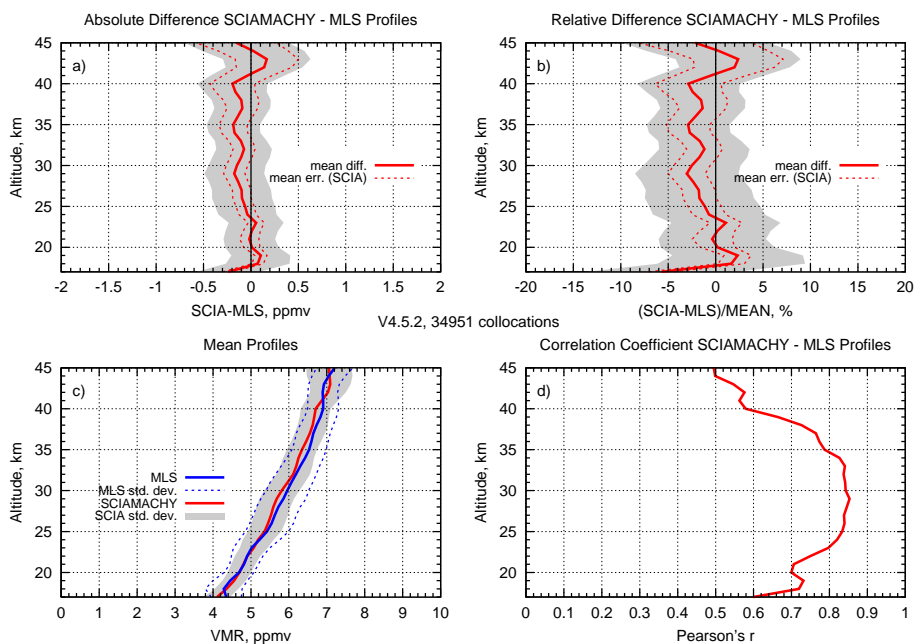
Figure 4. Same as Fig. 3, but for comparison of retrieved SCIAMACHY H$_2$O profiles with MLS data 2004–2012.
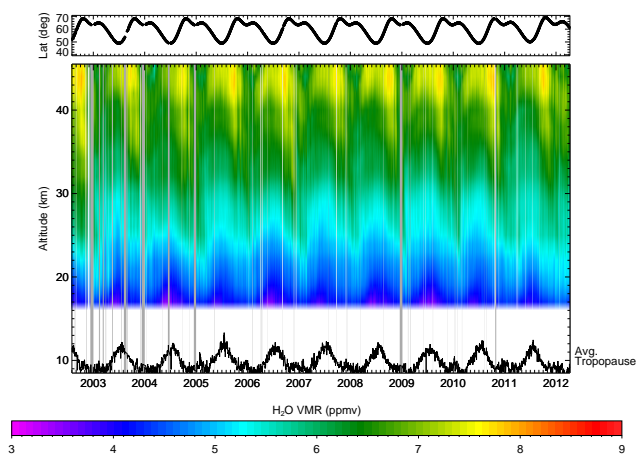
Figure 5. Time series of daily averaged SCIAMACHY H$_2$O VMR profiles from August 2002 to April 2012. In the top graph the latitudes of observations as function of time are shown. Grey vertical bars mask out times of reduced SCIAMACHY performance or missing data. The black curve at lower altitudes shows the average tropopause height.
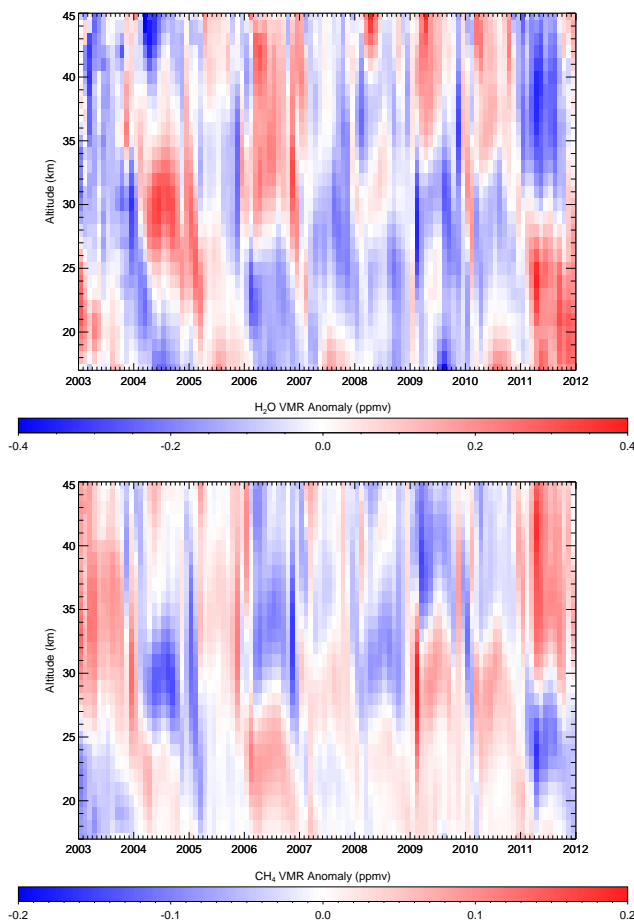
Figure 6. Time series of SCIAMACHY H_2O (top) and CH_4 (bottom) monthly VMR anomaly profiles from January 2003 to December 2011. The CH_4 plot is taken from Noël et al. (2016).

for each month. To avoid different weighting of different months we limit this analysis to the time interval 2003 to 2011, i.e. we use only years for which data for all months are available.

In Fig. 6 the time series of the H_2O and CH_4 anomalies are shown. There is a clear bi-annual structure visible in both data sets with opposite sign. As already mentioned in Noël et al. (2016), this structure is related to the Quasi-Biannual-Oscillation

5 (QBO), see e.g. Baldwin et al. (2001).

However, although the structures are quite similar, water vapour and methane variations show an inverted behaviour: Positive methane anomalies correspond to about twice as high negative water vapour anomalies and vice versa. This is in line with the assumption, that most of the water vapour is produced from methane via the net reaction (R2).

To investigate this further, Fig. 7 shows for some selected altitudes the water vapour anomalies as a function of time together

10 with the methane anomalies multiplied by −2. If water vapour would be produced solely via reaction (R2), both curves would
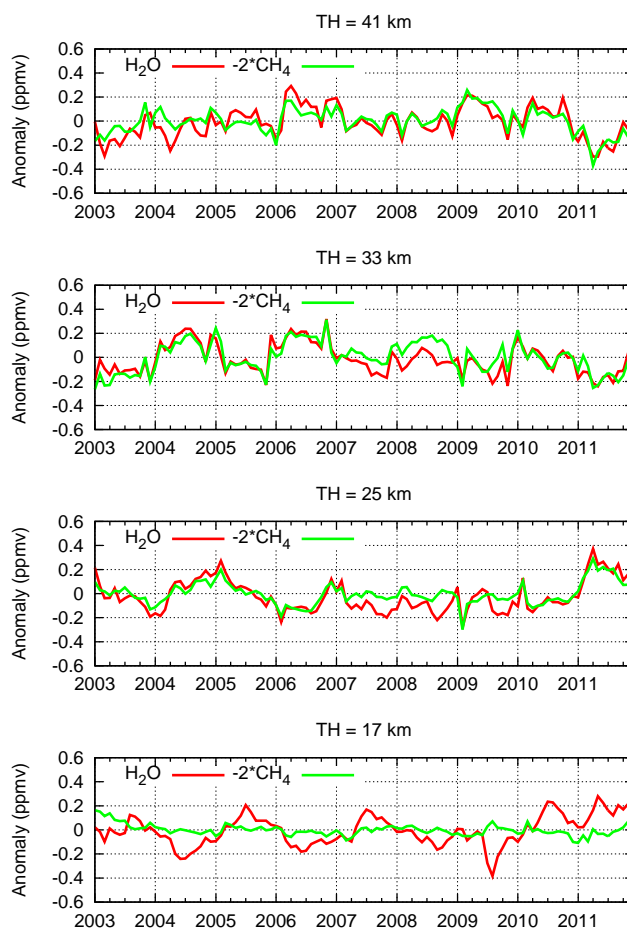
Figure 7. Time series of SCIAMACHY water vapour and methane anomalies at different altitudes. Methane data have been scaled by a factor -2.

be identical. This is in fact nearly the case for altitudes above about $25\,\mathrm{km}$, where the water vapour variations follow quite well the methane variation. At $17\,\mathrm{km}$, however, the methane anomaly does not vary much whereas the water vapour anomaly still shows a clear QBO signature, which is shifted in phase with respect to $25\,\mathrm{km}$.

The downward peak in the water vapour anomalies in the middle of 2009 is related to the eruption of the Sarychev volcano
5 on 12 June 2009 which reached these altitudes (Jégou et al., 2013). Note that this observed reduction of water vapour after the Sarychev eruption may be introduced by the remaining sensitivity of the retrieval method to aerosol. In the retrieval only spectrally broadband contributions of aerosols are considered, but there are also (second order) effects e.g. caused by the vertical integration of the signal over the field of view, which may play a role in case of large aerosol concentrations. This issue is still under investigation.

10 The relation to QBO is illustrated in Fig. 8 which shows SCIAMACHY methane and water vapour anomalies at $30\,\mathrm{km}$ altitude as a function of time in comparison to Singapore monthly mean stratospheric zonal wind at $10\,\mathrm{hPa}$ (corresponding to
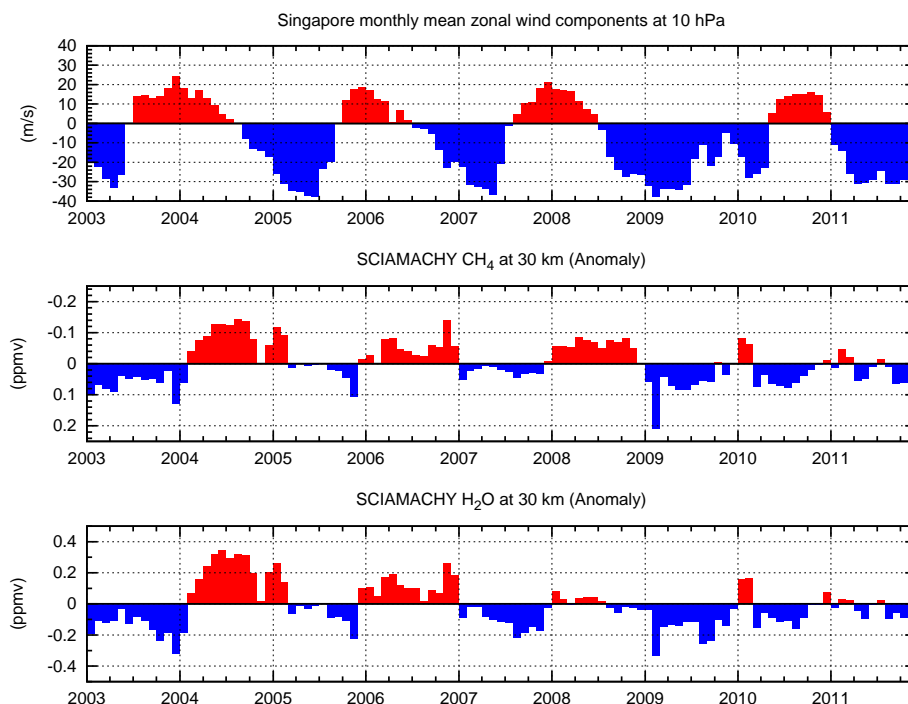
Figure 8. Time series of methane and water vapour anomalies at $30\,\mathrm{km}$ (middle and lower plots) and Singapore zonal wind at $10\,\mathrm{hPa}$, corresponding to about $30\,\mathrm{km}$ (top). Note that the vertical axis of the methane data is inverted.

about the same altitude), which is commonly used as proxy for the QBO (see e.g. Gebhardt et al., 2014). The Singapore wind data have been provided by Freie Universität Berlin (2014). Negative wind direction corresponds to Easterly winds (marked blue in Fig. 8), positive direction to Westerly winds (marked red). Water vapour negative and positive anomalies are also plotted in blue and red, respectively. For the methane plot, the vertical axis and colouring has been inverted, because an increase in

5   water vapour should correspond to a reduction of methane according to (R2).

Fig. 8 shows that water vapour and (inverted) methane anomalies follow the variation of the Singapore winds / QBO quite well, supporting that the changes are mainly affected by transport processes. The phase shift between stratospheric wind and SCIAMACHY data is related to the time delay caused by the transport of air from the tropics (where Singapore winds are measured) and the mid/high latitudes of the SCIAMACHY data. After about 2010 there are some differences between the

10 wind data and the SCIAMACHY results. Especially, the positive anomaly in the wind data around 2010/2011 is only hardly visible in the methane and water vapour data. On the other hand, positive anomalies of water vapour and (inverted) methane are quite strong at the begin of the time series. Possible reasons for this are currently unclear; maybe this is related to trends in the SCIAMACHY data (see below), but this requires further investigations.
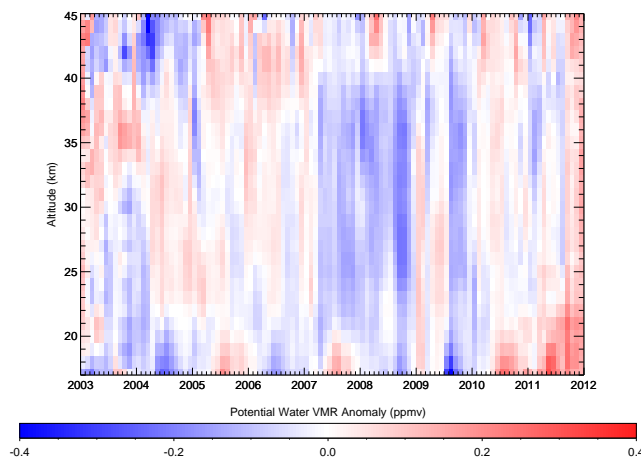
Figure 9. Potential water anomalies derived from combination of SCIAMACHY H_2O and CH_4 anomalies (Fig. 6).

3.4 Potential water

To further investigate the temporal variabilities a time series has been derived by adding to the water vapour VMR anomalies two times the methane anomalies. As mentioned above this combination, referred to as potential water (Nassar et al., 2005), is assumed to be conserved if water vapour is solely produced from methane oxidation, and temporal variations of this quantity
5   can be related to changes in transport or additional sources and sinks. The result is displayed in Fig. 9.

Below about 20 km the bi-annual structure of the QBO is visible. After about 2010 there seems to be an additional increase of potential water, which is transported upwards. From the methane and water vapour time series shown in Fig. 7 it is evident that most of these changes are due to changing water vapour VMRs. The negative values in the second half of 2009 are related to the Sarychev eruption, as explained before.
10   Between 20 and 40 km the vertical profile of the potential water anomaly is especially in summer (i.e. at lower latitudes) rather constant. In winter (corresponding to higher latitudes) sometimes larger variability is observed, possibly due to influences of the polar vortex. In 2003 and the first months of 2004, patterns are more patchy due to the different vertical sampling of measurements at this time (see also Noël et al., 2016). In this time interval, positive anomalies occur around 35 km, negative anomalies above and below. Between about 2004 and 2007 potential water anomalies are typically positive whereas from 2007
15   to 2009 or 2010 they are mainly negative, later on they tend to be positive again. This suggests a periodicity of about 5 to 6 years, but due to the shortness of the time series it is not possible to confirm this.

Above 40 km the variability of the potential water anomaly is quite high. This may be related to the larger uncertainties of the ONPD data at higher altitudes.
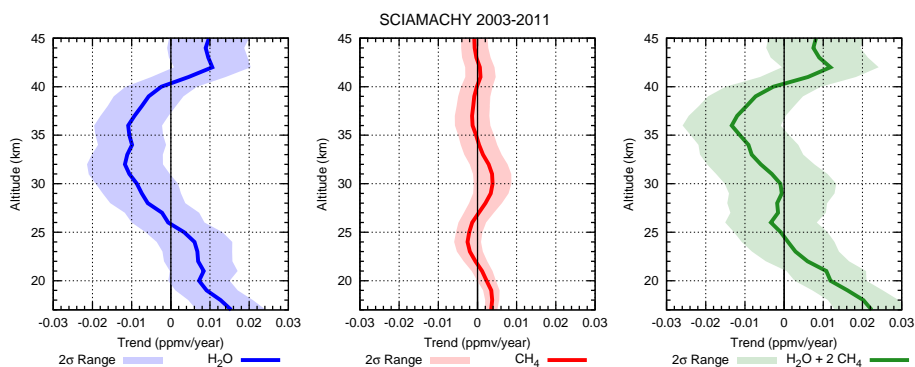
Figure 10. Calculated VMR trends of H_2O (blue; left) and CH_4 (red; middle) from 2003 to 2011 as function of altitude. Methane data are from Noël et al. (2016). Right plot: Potential water trend derived from the combination of H_2O and CH_4 trends.

3.5 Trends

A linear trend model has been fitted to the water vapour anomalies at each altitude similar to what has been applied in the earlier methane study, see Noël et al. (2016). The trend profiles are displayed in Fig. 10.

The derived water vapour trends (left plot) are positive at altitudes below about 25 km, reaching a maximum value of about $0.015 \, \mathrm{ppmv \, year^{-1}}$ at 17 km. Between about 25 and 40 km the water vapour trends are negative and up to about -$0.01 \, \mathrm{ppmv \, year^{-1}}$. The 2σ uncertainty ranges also plotted indicate that the water vapour trends are not significant in a statistical sense at altitudes above 37 km and between 20 and 30 km where the trend switches sign. A positive trend in lower stratospheric water vapour during the time interval considered in this study has been observed by Urban et al. (2014) and Weigel et al. (2016) mainly in the tropics. As already discussed in Noël et al. (2016) methane trends are also not significant except for the lowest altitudes, where they are in general agreement with tropospheric trends. However, it should be noted that errors of the data and autocorrelation of noise have not been considered in the trend fits, which might affect the trend errors.

The potential water vapour trend is the sum of the water vapour trend and two times the methane trend. This is an estimate an estimate for water vapour changes or methane changes not related to the stratospheric production of water vapour by methane. If potential water is conserved, this trend should be zero. The potential water trend profile is shown in the right plot of Fig. 10. The error of the potential water trend has been derived via propagation of the errors of the methane and water vapour trends. Considering this error, the combined trend above about 20 km is in a statistical sense not significant, meaning that the assumption that all water vapour is produced from methane via the net reaction (R2) is not disproved by the measurements. This is especially the case between 25 and 30 km where the trend itself is close to zero. At the lower altitudes, a significant deviation of the potential water trend from zero is observed (up to about $0.02 \, \mathrm{ppmv \, year^{-1}}$).

4 Discussion

The findings of the previous section can be summarised as follows:
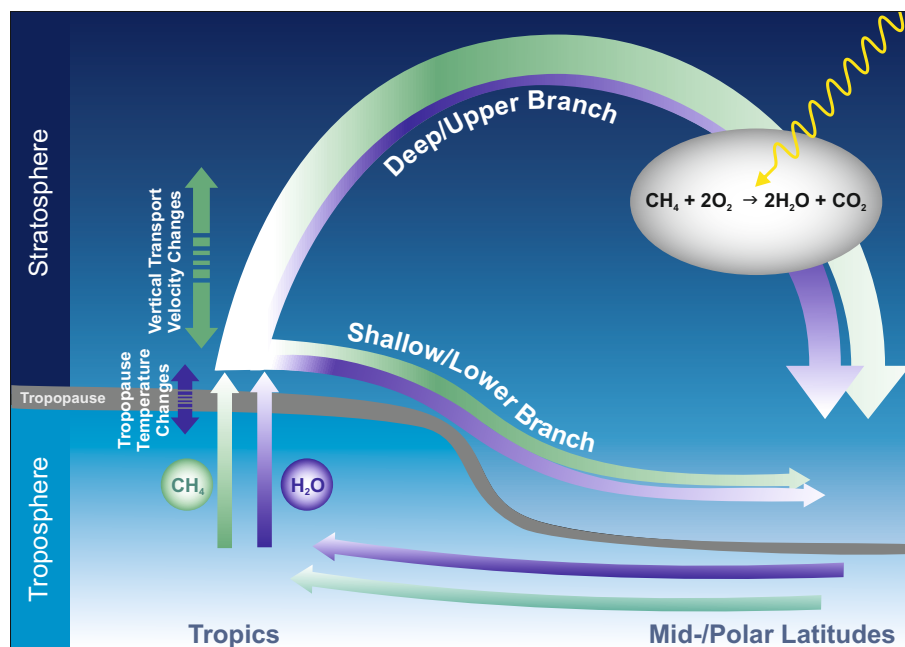
Figure 11. Simplified schematic view of transport pathways within the Brewer-Dobson circulation.

- – Water vapour and methane time series and trends look different above and below about $20\,\mathrm{km}$.

- – In the upper altitudes both water vapour and methane time series show a pronounced QBO signature.

- – In the lower stratosphere, QBO signature is only visible in the water vapour data.

- – There is a phase shift in the water vapour QBO signal between upper and lower altitudes.

5 – Potential water, the combination of methane and water vapour VMRs, is essentially conserved at upper altitudes except for some short-term events and a longer-term variation with a period of about 5–6 years.

- – The QBO signal is also visible in the potential water data at lower altitudes until about 2009/2010; after that potential water increases slowly.

These observations can be explained by a separation of the stratosphere into two vertical regimes. The lower region is
10 mainly affected by the shallow (or lower) branch of the Brewer-Dobson circulation (see e.g. Butchart, 2014, and references therein), whereas in the upper part the deep (or upper) branch of the Brewer-Dobson circulation dominates, see also Fig. 11. According to the data of the present study, this separation occurs at about $20\,\mathrm{km}$; however it has to be kept in mind that this is an approximated value and that the vertical resolution of the SCIAMACHY solar occultation data is about $4\,\mathrm{km}$.

In the lower region, variability is determined by water vapour variations due to QBO effects on tropopause temperature and/or stratospheric transport and due to tropospheric methane variations; above, water vapour is mainly produced from methane oxidation and potential water anomalies are more homogeneous with altitude and change on longer time scales.

Water vapour and methane below 20 km are therefore dominated by the variations imprinted on them from their tropospheric

5 sources especially during their vertical transport into the stratosphere at tropical regions. The amount of water vapour entering the tropical stratosphere is related to the tropopause temperature which varies with QBO, see e.g. Fueglistaler and Haynes (2005). This is not the case for methane, which could explain the missing QBO signature in the methane time series at 17 km (Fig. 7).

The missing balance between methane and water vapour at lower altitudes is in fact not surprising, because the photochem-

10 ical processes involved in the conversion of methane to water vapour are less effective there since less UV radiation reaches these altitudes (le Texier et al., 1988). Furthermore, since the transport via the shallow branch is comparably fast (less than about one year from the entry point in the tropics to mid-latitudes, see Birner and Bönisch, 2011) the balance between water vapour and methane is also not reached in the extratropical lowermost stratosphere. This could explain the phase shift in the water vapour QBO signal between 25 and 17 km (Fig. 7) and is in line with measurements of age of air by e.g. Haenel et al.

15 (2015) which show that the air at 17 km is younger than the air above.

Schneising et al. (2011) estimated for the time interval 2007 to 2009 a tropospheric increase of methane of about 8 ppbv year^{-1} following a period of no significant change from 2003 to 2007. Considering a delay between the tropospheric and a possible stratospheric trend related to the age of air (about 2–3 years since emission at 17 km according to Haenel et al., 2015), this could explain the increase of potential water at lower altitudes after 2009/2010 shown in Fig. 9. Until end of 2011 the positive

20 potential water anomaly extends to higher altitudes. This is in agreement with the increasing age of air at higher altitudes. However, from the current data set an additional influence of varying tropospheric water vapour input on the observed increase of potential water cannot be ruled out.

Above 20 km, in the region of the deep branch of the Brewer-Dobson circulation, air is older such that the conversion process from methane to water vapour has reached an equilibrium, variations of both gases are in phase and potential water is

25 essentially conserved (Fig. 7). A remaining open issue is the QBO signal observed in both methane and water vapour at higher stratospheric altitudes. The conservation of potential water indicates that at these altitudes water vapour changes are mainly related to changes of methane. Therefore the QBO signal has to be carried by methane, but as can be seen at lower altitudes the methane entering the stratosphere is not varied by QBO. The QBO signature in the upper altitude data can be explained by a QBO-related modulation of the transport to higher latitudes via the deep branch of the Brewer-Dobson circulation, similar to

30 the variation in tropical aerosol extinction coefficients as seen by Brinkhoff et al. (2015) at 30 km. Also Randel et al. (1998) observed a QBO signal in tropical methane from HALOE measurements on UARS above about 35 km but not below, correlated with the residual mean wind circulation. This is also in line with results from e.g. Niwano et al. (2003) and Minschwaner et al. (2016) who determined vertical transport velocity in the tropics from HALOE and MLS measurements, respectively, and confirmed a variation with QBO.

5 Conclusions

A new stratospheric water vapour data set based on SCIAMACHY solar occultation measurements is available. It covers the latitude range between about 50 and 70°N and the altitude range from 17 to 45 km. It has been generated in a similar way as the corresponding methane product (Noël et al., 2016) resulting in a consistent data set. Comparisons with independent data

5   indicate an accuracy of the water vapour profiles of about 5%. Between 2003 and 2011 a significant positive water vapour trend is observed at altitudes below 20 km (0.015 ppmv year^{-1} at 17 km). On the other hand, a significant negative water vapour trend of about -0.01 ppmv year^{-1} is derived for the altitude range 30–37 km.

Variations in water vapour are clearly correlated with those of methane. A QBO signature is visible in both water vapour and methane anomaly time series, showing that transport from the tropics affects essentially the whole altitude range under

10   investigation in this study.

The analysis of the combined water vapour and methane data sets reveals, that potential water, the sum of water vapour VMR and two time methane VMR, seems to be overall conserved between about 20 and 40–45 km. However, potential water is not constant over time. In addition to short term fluctuations a variation on a timescale of 5–6 years is observed, which needs further investigation.

15   At altitudes below about 20 km the QBO signature is only visible in water vapour but not in methane data. As a consequence, potential water also shows a significant QBO variation, but also a continuous increase after about 2009.

We explain this behaviour by a separation of the stratosphere into two regimes: Altitudes above about 20 km are fed via the deep branch of the Brewer-Dobson circulation, and water vapour is essentially produced from methane oxidation. At altitudes below water vapour and methane have been transported from the tropics to higher latitudes via the shallow branch of the

20   Brewer-Dobson circulation. The rise of tropospheric methane after 2007 reaches these lower stratospheric altitudes with a delay of about 2 years, resulting – possibly in combination with changes of water vapour – in the observed increase of potential water after 2009.

Data availability. SCIAMACHY Level 1b data are available from ESA (https://earth.esa.int) after registration. All SCIAMACHY ONPD data V4.5.2 are available on request from S. Noël. The methane product V4.5.2 is also provided via the GHG-CCI web site http://www.

25   esa-ghg-cci.org/ and accessible after registration.

Competing interests. The authors declare that they have no conflict of interest.

Acknowledgements. The Atmospheric Chemistry Experiment (ACE), also known as SCISAT, is a Canadian-led mission mainly supported by the Canadian Space Agency and the Natural Sciences and Engineering Research Council of Canada. The MLS data used in this research were produced by the Jet Propulsion Laboratory, California Institute of Technology under contract with the National Aeronautics and

Space Adminstration (https://urs.earthdata.nasa.gov/, https://mls.jpl.nasa.gov/). The European Centre for Medium Range Weather Forecasts (ECMWF) provided the ERA Interim meteorological data used in this study. FU Berlin provided Singapore winds data. Geoffrey Toon of the NASA Jet Propulsion Laboratory is acknowledged for providing the empirical solar line list used in the retrieval. This work has been funded by DLR Space Agency (Germany), the ESA GHG-CCI and by the University of Bremen.

References

Baldwin, M. P., Gray, L. J., Dunkerton, T. J., Hamilton, K., Haynes, P. H., Randel, W. J., Holton, J. R., Alexander, M. J., Hirota, I., Horinouchi, T., Jones, D. B. A., Kinnersley, J. S., Marquardt, C., Sato, K., and Takahashi, M.: The quasi-biennial oscillation, Reviews of Geophysics, 39, 179–229, https://doi.org/10.1029/1999RG000073, http://dx.doi.org/10.1029/1999RG000073, 2001.

5 Bernath, P. F., McElroy, C. T., Abrams, M. C., Boone, C. D., Butler, M., Camy-Peyret, C., Carleer, M., Clerbaux, C., Coheur, P.-F., Colin, R., DeCola, P., DeMazière, M., Drummond, J. R., Dufour, D., Evans, W. F. J., Fast, H., Fussen, D., Gilbert, K., Jennings, D. E., Llewellyn, E. J., Lowe, R. P., Mahieu, E., McConnell, J. C., McHugh, M., McLeod, S. D., Michaud, R., Midwinter, C., Nassar, R., Nichitiu, F., Nowlan, C., Rinsland, C. P., Rochon, Y. J., Rowlands, N., Semeniuk, K., Simon, P., Skelton, R., Sloan, J. J., Soucy, M.-A., Strong, K., Tremblay, P., Turnbull, D., Walker, K. A., Walkty, I., Wardle, D. A., Wehrle, V., Zander, R., and Zou, J.: Atmospheric Chemistry
10 Experiment (ACE): Mission overview, Geophys. Res. Lett., 32, L15S01, https://doi.org/10.1029/2005GL022386, 2005.

Birner, T. and Bönisch, H.: Residual circulation trajectories and transit times into the extratropical lowermost stratosphere, Atmos. Chem. Phys., 11, 817–827, https://doi.org/10.5194/acp-11-817-2011, https://www.atmos-chem-phys.net/11/817/2011/, 2011.

Bovensmann, H., Burrows, J. P., Buchwitz, M., Frerick, J., Noël, S., Rozanov, V. V., Chance, K. V., and Goede, A. H. P.: SCIAMACHY — Mission Objectives and Measurement Modes, J. Atmos. Sci., 56, 127–150, 1999.

15 Brinkhoff, L. A., Rozanov, A., Hommel, R., von Savigny, C., Ernst, F., Bovensmann, H., and Burrows, J. P.: Ten-Year SCIAMACHY Stratospheric Aerosol Data Record: Signature of the Secondary Meridional Circulation Associated with the Quasi-Biennial Oscillation, in: Towards an Interdisciplinary Approach in Earth System Science: Advances of a Helmholtz Graduate Research School, edited by Lohmann, G., Meggers, H., Unnithan, V., Wolf-Gladrow, D., Notholt, J., and Bracher, A., pp. 49–58, Springer International Publishing, https://doi.org/10.1007/978-3-319-13865-7_6, https://doi.org/10.1007/978-3-319-13865-7_6, 2015.

20 Buchwitz, M., Schneising, O., Reuter, M., Heymann, J., Krautwurst, S., Bovensmann, H., Burrows, J. P., Boesch, H., Parker, R. J., Somkuti, P., Detmers, R. G., Hasekamp, O. P., Aben, I., Butz, A., Frankenberg, C., and Turner, A. J.: Satellite-derived methane hotspot emission estimates using a fast data-driven method, Atmos. Chem. Phys., 17, 5751–5774, https://doi.org/10.5194/acp-17-5751-2017, http://www.atmos-chem-phys.net/17/5751/2017/, 2017.

Burrows, J. P., Weber, M., Buchwitz, M., Rozanov, V., Ladstätter-Weißenmayer, A., Richter, A., de Beek, R., Hoogen, R., Bramstedt, K.,
25 Eichmann, K.-U., Eisinger, M., and Perner, D.: The Global Ozone Monitoring Experiment (GOME): Mission Concept and First Scientific Results, J. Atmos. Sci., 56, 151–175, 1999.

Butchart, N.: The Brewer-Dobson circulation, Rev. Geophys., 52, 157–184, https://doi.org/10.1002/2013RG000448, http://dx.doi.org/10.1002/2013RG000448, 2014.

Carr, E. S., Harwood, R. S., Mote, P. W., Peckham, G. E., Suttie, R. A., Lahoz, W. A., O'Neill, A., Froidevaux, L., Jarnot, R. F., Read, W. G.,
30 Waters, J. W., and Swinbank, R.: Tropical stratospheric water vapor measured by the Microwave Limb Sounder (MLS), Geophys. Res. Lett., 22, 691–694, https://doi.org/10.1029/95GL00626, http://dx.doi.org/10.1029/95GL00626, 1995.

Coldewey-Egbers, M., Weber, M., Lamsal, L. N., de Beek, R., Buchwitz, M., and Burrows, J. P.: Total ozone retrieval from GOME UV spectral data using the weighting function DOAS approach, Atmospheric Chemistry and Physics, 5, 1015–1025, https://doi.org/10.5194/acp-5-1015-2005, http://www.atmos-chem-phys.net/5/1015/2005/, 2005.

35 Dee, D. P., Uppala, S. M., Simmons, A. J., Berrisford, P., Poli, P., Kobayashi, S., Andrae, U., Balmaseda, M. A., Balsamo, G., Bauer, P., Bechtold, P., Beljaars, A. C. M., van de Berg, L., Bidlot, J., Bormann, N., Delsol, C., Dragani, R., Fuentes, M., Geer, A. J., Haimberger, L., Healy, S. B., Hersbach, H., Hólm, E. V., Isaksen, L., Kållberg, P., Köhler, M., Matricardi, M., McNally, A. P., Monge-Sanz,

B. M., Morcrette, J.-J., Park, B.-K., Peubey, C., de Rosnay, P., Tavolato, C., Thépaut, J.-N., and Vitart, F.: The ERA-Interim reanalysis: configuration and performance of the data assimilation system, Quart. J. Royal Met. Soc., 137, 553–597, https://doi.org/10.1002/qj.828, http://dx.doi.org/10.1002/qj.828, 2011.

Dhomse, S., Weber, M., and Burrows, J.: The relationship between tropospheric wave forcing and tropical lower stratospheric water vapor, Atmos. Chem. Phys., 8, 471–480, https://doi.org/10.5194/acp-8-471-2008, https://www.atmos-chem-phys.net/8/471/2008/, 2008.

Fischer, H., Birk, M., Blom, C., Carli, B., Carlotti, M., von Clarmann, T., Delbouille, L., Dudhia, A., Ehhalt, D., Endemann, M., Flaud, J. M., Gessner, R., Kleinert, A., Koopman, R., Langen, J., López-Puertas, M., Mosner, P., Nett, H., Oelhaf, H., Perron, G., Remedios, J., Ridolfi, M., Stiller, G., and Zander, R.: MIPAS: an instrument for atmospheric and climate research, Atmos. Chem. Phys., 8, 2151–2188, http://www.atmos-chem-phys.net/8/2151/2008/, 2008.

Freie Universität Berlin: Die Quasi-Biennial-Oszillation (QBO) Datenreihe, Fachbereich Geowissenschaften / Institut für Meteorologie, AG Atmosphärendynamik, http://www.geo.fu-berlin.de/met/ag/strat/produkte/qbo/index.html, downloaded 9 July, 2014.

Fueglistaler, S. and Haynes, P. H.: Control of interannual and longer-term variability of stratospheric water vapor, J. Geophys. Res. Atmos., 110, https://doi.org/10.1029/2005JD006019, http://dx.doi.org/10.1029/2005JD006019, d24108, 2005.

Gebhardt, C., Rozanov, A., Hommel, R., Weber, M., Bovensmann, H., Burrows, J. P., Degenstein, D., Froidevaux, L., and Thompson, A. M.: Stratospheric ozone trends and variability as seen by SCIAMACHY from 2002 to 2012, Atmos. Chem. Phys., 14, 831–846, https://doi.org/10.5194/acp-14-831-2014, https://www.atmos-chem-phys.net/14/831/2014/, 2014.

Gordley, L. L., Hervig, M. E., Fish, C., Russell, J. M., Bailey, S., Cook, J., Hansen, S., Shumway, A., Paxton, G., Deaver, L., Marshall, T., Burton, J., Magill, B., Brown, C., Thompson, E., and Kemp, J.: The solar occultation for ice experiment, J. Atmos. Sol.-Terr. Phys., 71, 300 – 315, https://doi.org/http://dx.doi.org/10.1016/j.jastp.2008.07.012, http://www.sciencedirect.com/science/article/pii/S136468260800206X, global Perspectives on the Aeronomy of the Summer Mesopause Region, 2009.

Gottwald, M. and Bovensmann, H., eds.: SCIAMACHY - Exploring the Changing Earth's Atmosphere, Springer Dordrecht Heidelberg London New York, https://doi.org/10.1007/978-90-481-9896-2, 2011.

Haenel, F. J., Stiller, G. P., von Clarmann, T., Funke, B., Eckert, E., Glatthor, N., Grabowski, U., Kellmann, S., Kiefer, M., Linden, A., and Reddmann, T.: Reassessment of MIPAS age of air trends and variability, Atmos. Chem. Phys., 15, 13 161–13 176, https://doi.org/10.5194/acp-15-13161-2015, https://www.atmos-chem-phys.net/15/13161/2015/, 2015.

Holton, J. R. and Gettelman, A.: Horizontal transport and the dehydration of the stratosphere, Geophys. Res. Lett., 28, 2799–2802, https://doi.org/10.1029/2001GL013148, http://dx.doi.org/10.1029/2001GL013148, 2001.

Jégou, F., Berthet, G., Brogniez, C., Renard, J.-B., François, P., Haywood, J. M., Jones, A., Bourgeois, Q., Lurton, T., Auriol, F., Godin-Beekmann, S., Guimbaud, C., Krysztofiak, G., Gaubicher, B., Chartier, M., Clarisse, L., Clerbaux, C., Balois, J. Y., Verwaerde, C., and Daugeron, D.: Stratospheric aerosols from the Sarychev volcano eruption in the 2009 Arctic summer, Atmos. Chem. Phys., 13, 6533–6552, https://doi.org/10.5194/acp-13-6533-2013, http://www.atmos-chem-phys.net/13/6533/2013/, 2013.

Juckes, M. N.: An annual cycle of long lived stratospheric gases from MIPAS, Atmos. Chem. Phys., 7, 1879–1897, https://doi.org/10.5194/acp-7-1879-2007, https://www.atmos-chem-phys.net/7/1879/2007/, 2007.

Laeng, A., Plieninger, J., von Clarmann, T., Grabowski, U., Stiller, G., Eckert, E., Glatthor, N., Haenel, F., Kellmann, S., Kiefer, M., Linden, A., Lossow, S., Deaver, L., Engel, A., Hervig, M., Levin, I., McHugh, M., Noël, S., Toon, G., and Walker, K.: Validation of MIPAS IMK/IAA methane profiles, Atmos. Meas. Tech., 8, 5251–5261, https://doi.org/10.5194/amt-8-5251-2015, http://www.atmos-meas-tech.net/8/5251/2015/, 2015.

Lambert, A., Read, W. G., Livesey, N. J., Santee, M. L., Manney, G. L., Froidevaux, L., Wu, D. L., Schwartz, M. J., Pumphrey, H. C., Jimenez, C., Nedoluha, G. E., Cofield, R. E., Cuddy, D. T., Daffer, W. H., Drouin, B. J., Fuller, R. A., Jarnot, R. F., Knosp, B. W., Pickett, H. M., Perun, V. S., Snyder, W. V., Stek, P. C., Thurstans, R. P., Wagner, P. A., Waters, J. W., Jucks, K. W., Toon, G. C., Stachnik, R. A., Bernath, P. F., Boone, C. D., Walker, K. A., Urban, J., Murtagh, D., Elkins, J. W., and Atlas, E.: Validation of the Aura Microwave Limb Sounder middle atmosphere water vapor and nitrous oxide measurements, J. Geophys. Res. Atmos., 112, n/a–n/a, https://doi.org/10.1029/2007JD008724, http://dx.doi.org/10.1029/2007JD008724, d24S36, 2007.

le Texier, H., Solomon, S., and Garcia, R. R.: The role of molecular hydrogen and methane oxidation in the water vapour budget of the stratosphere, Quart. J. Royal Met. Soc., 114, 281–295, https://doi.org/10.1002/qj.49711448002, http://dx.doi.org/10.1002/qj.49711448002, 1988.

Lossow, S., Khosrawi, F., Nedoluha, G. E., Azam, F., Bramstedt, K., Burrows, Dinelli, B. M., Eriksson, P., Espy, P. J., García-Comas, M., Gille, J. C., Kiefer, M., Noël, S., Raspollini, P., Read, W. G., Rosenlof, K. H., Rozanov, A., Sioris, C. E., Stiller, G. P., Walker, K. A., and Weigel, K.: The SPARC water vapour assessment II: comparison of annual, semi-annual and quasi-biennial variations in stratospheric and lower mesospheric water vapour observed from satellites, Atmos. Meas. Tech., 10, 1111–1137, https://doi.org/10.5194/amt-10-1111-2017, http://www.atmos-meas-tech.net/10/1111/2017/, 2017.

Minschwaner, K., Su, H., and Jiang, J. H.: The upward branch of the Brewer-Dobson circulation quantified by tropical stratospheric water vapor and carbon monoxide measurements from the Aura Microwave Limb Sounder, J. Geophys. Res. Atmos., 121, 2790–2804, https://doi.org/10.1002/2015JD023961, http://dx.doi.org/10.1002/2015JD023961, 2015JD023961, 2016.

Nassar, R., Bernath, P. F., Boone, C. D., Manney, G. L., McLeod, S. D., Rinsland, C. P., Skelton, R., and Walker, K. A.: Stratospheric abundances of water and methane based on ACE-FTS measurements, Geophys. Res. Lett., 32, https://doi.org/10.1029/2005GL022383, http://dx.doi.org/10.1029/2005GL022383, l15S04, 2005.

Niwano, M., Yamazaki, K., and Shiotani, M.: Seasonal and QBO variations of ascent rate in the tropical lower stratosphere as inferred from UARS HALOE trace gas data, J. Geophys. Res. Atmos., 108, n/a–n/a, https://doi.org/10.1029/2003JD003871, http://dx.doi.org/10.1029/2003JD003871, 4794, 2003.

Noël, S., Bramstedt, K., Rozanov, A., Bovensmann, H., and Burrows, J. P.: Water vapour profiles from SCIAMACHY solar occultation measurements derived with an onion peeling approach, Atmos. Meas. Tech., 3, 523–535, http://www.atmos-meas-tech.net/3/523/2010/, 2010.

Noël, S., Bramstedt, K., Hilker, M., Liebing, P., Plieninger, J., Reuter, M., Rozanov, A., Sioris, C. E., Bovensmann, H., and Burrows, J. P.: Stratospheric CH_4 and CO_2 profiles derived from SCIAMACHY solar occultation measurements, Atmos. Meas. Tech., 9, 1485–1503, https://doi.org/10.5194/amt-9-1485-2016, http://www.atmos-meas-tech.net/9/1485/2016/, 2016.

Payan, S., Camy-Peyret, C., Oelhaf, H., Wetzel, G., Maucher, G., Keim, C., Pirre, M., Huret, N., Engel, A., Volk, M. C., Kuellmann, H., Kuttippurath, J., Cortesi, U., Bianchini, G., Mencaraglia, F., Raspollini, P., Redaelli, G., Vigouroux, C., De Maziére, M., Mikuteit, S., Blumenstock, T., Velazco, V., Notholt, J., Mahieu, E., Duchatelet, P., Smale, D., Wood, S., Jones, N., Piccolo, C., Payne, V., Bracher, A., Glatthor, N., Stiller, G., Grunow, K., Jeseck, P., Te, Y., and Butz, A.: Validation of version-4.61 methane and nitrous oxide observed by MIPAS, Atmos. Chem. Phys., 9, 413–442, https://doi.org/10.5194/acp-9-413-2009, http://www.atmos-chem-phys.net/9/413/2009/, 2009.

Payne, V., Dudhia, A., and Piccolo, C.: Analysis of Water Vapour and Methane from the MIPAS Satellite Instrument, in: Proceedings of the 2004 Envisat & ERS Symposium 6–10 September 2004, Salzburg, Austria, edited by Lacoste, H. and Ouwehand, L., vol. 572 of *ESA Special Publication*, 2005.

Perner, D. and Platt, U.: Detection of Nitrous Acid in the Atmosphere by Differential Optical Absorption, Geophys. Res. Lett., 6, 917–920, 1979.

Plieninger, J., Laeng, A., Lossow, S., von Clarmann, T., Stiller, G. P., Kellmann, S., Linden, A., Kiefer, M., Walker, K. A., Noël, S., Hervig, M. E., McHugh, M., Lambert, A., Urban, J., Elkins, J. W., and Murtagh, D.: Validation of revised methane and nitrous oxide profiles from MIPAS–ENVISAT, Atmos. Meas. Tech., 9, 765–779, https://doi.org/10.5194/amt-9-765-2016, http://www.atmos-meas-tech.net/9/765/2016/, 2016.

Randel, W. J. and Jensen, E. J.: Physical processes in the tropical tropopause layer and their roles in a changing climate, Nature Geosci., 6, 169–176, https://doi.org/10.1038/ngeo1733, 2013.

Randel, W. J., Wu, F., Russell, III, J. M., Roche, A., and Waters, J. W.: Seasonal Cycles and QBO Variations in Stratospheric CH_4 and H_2O Observed in UARS HALOE Data., J. Atmos. Sci., 55, 163–185, https://doi.org/10.1175/1520-0469(1998)055<0163:SCAQVI>2.0.CO;2, 1998.

Randel, W. J., Wu, F., Oltmans, S. J., Rosenlof, K., and Nedoluha, G. E.: Interannual Changes of Stratospheric Water Vapor and Correlations with Tropical Tropopause Temperatures, J. Atmos. Sci., 61, 2133–2148, https://doi.org/10.1175/1520-0469(2004)061<2133:ICOSWV>2.0.CO;2, https://doi.org/10.1175/1520-0469(2004)061<2133:ICOSWV>2.0.CO;2, 2004.

Randel, W. J., Wu, F., Vömel, H., Nedoluha, G. E., and Forster, P.: Decreases in stratospheric water vapor after 2001: Links to changes in the tropical tropopause and the Brewer-Dobson circulation, J. Geophys. Res. Atmos., 111, https://doi.org/10.1029/2005JD006744, http://dx.doi.org/10.1029/2005JD006744, d12312, 2006.

Read, W. G., Wu, D. L., Waters, J. W., and Pumphrey, H. C.: Dehydration in the tropical tropopause layer: Implications from the UARS Microwave Limb Sounder, J. Geophys. Res. Atmos., 109, https://doi.org/10.1029/2003JD004056, http://dx.doi.org/10.1029/2003JD004056, d06110, 2004.

Rong, P. P., Russell, J. M., Marshall, B. T., Siskind, D. E., Hervig, M. E., Gordley, L. L., Bernath, P. F., and Walker, K. A.: Version 1.3 AIM SOFIE measured methane (CH_4): Validation and seasonal climatology, J. Geophys. Res. Atmos., 121, 13,158–13,179, https://doi.org/10.1002/2016JD025415, http://dx.doi.org/10.1002/2016JD025415, 2016JD025415, 2016.

Rosenlof, K. H.: Transport Changes Inferred from HALOE Water and Methane Measurements, J. Met. Soc. Japan, 80, 831–848, https://doi.org/10.2151/jmsj.80.831, 2002.

Rozanov, V. V., Rozanov, A. V., Kokhanovsky, A. A., and Burrows, J. P.: Radiative transfer through terrestrial atmosphere and ocean: Software package SCIATRAN, J. Quant. Spectr. Rad. Transf., 133, 13–71, https://doi.org/10.1016/j.jqsrt.2013.07.004, http://www.sciencedirect.com/science/article/pii/S0022407313002872, 2014.

Russell, III, J. M. and Drayson, S. R.: The Inference of Atmospheric Ozone Using Satellite Horizon Measurements in the 1042 cm^{-1} Band, J. Atmos. Sci., 29, 376–390, 1972.

Russell, III, J. M., Gordley, L. L., Park, J. H., Drayson, S. R., Hesketh, W. D., Cicerone, R. J., Tuck, A. F., Frederick, J. E., Harries, J. E., and Crutzen, P. J.: The Halogen Occultation Experiment, J. Geophys. Res., 98, 10 777–10 797, 1993.

Schneising, O., Buchwitz, M., Reuter, M., Heymann, J., Bovensmann, H., and Burrows, J. P.: Long-term analysis of carbon dioxide and methane column-averaged mole fractions retrieved from SCIAMACHY, Atmos. Chem. Phys., 11, 2863–2880, https://doi.org/10.5194/acp-11-2863-2011, http://www.atmos-chem-phys.net/11/2863/2011/, 2011.

Seinfeld, J. and Pandis, S.: Atmospheric Chemistry and Physics: From Air Pollution to Climate Change, Wiley, 2 edn., 2006.

Urban, J., Lossow, S., Stiller, G., and Read, W.: Another Drop in Water Vapor, Eos, 95, 245–246, https://doi.org/10.1002/2014EO270001, http://dx.doi.org/10.1002/2014EO270001, 2014.

Waters, J. W., Froidevaux, L., Harwood, R. S., Jarnot, R. F., Pickett, H. M., Read, W. G., Siegel, P. H., Cofield, R. E., Filipiak, M. J., Flower, D. A., Holden, J. R., Lau, G. K., Livesey, N. J., Manney, G. L., Pumphrey, H. C., Santee, M. L., Wu, D. L., Cuddy, D. T., Lay, R. R., Loo, M. S., Perun, V. S., Schwartz, M. J., Stek, P. C., Thurstans, R. P., Boyles, M. A., Chandra, K. M., Chavez, M. C., Chen, G.-S., Chudasama, B. V., Dodge, R., Fuller, R. A., Girard, M. A., Jiang, J. H., Jiang, Y., Knosp, B. W., LaBelle, R. C., Lam, J. C., Lee, K. A., Miller, D.,

5   Oswald, J. E., Patel, N. C., Pukala, D. M., Quintero, O., Scaff, D. M., Snyder, W. V., Tope, M. C., Wagner, P. A., and Walch, M. J.: The Earth observing system microwave limb sounder (EOS MLS) on the aura Satellite, Trans. Geosci. Remote Sens., 44, 1075–1092, https://doi.org/10.1109/TGRS.2006.873771, 2006.

Weigel, K., Rozanov, A., Azam, F., Bramstedt, K., Damadeo, R., Eichmann, K.-U., Gebhardt, C., Hurst, D., Kraemer, M., Lossow, S., Read, W., Spelten, N., Stiller, G. P., Walker, K. A., Weber, M., Bovensmann, H., and Burrows, J. P.: UTLS water vapour from

10   SCIAMACHY limb measurements V3.01 (2002–2012), Atmos. Meas. Tech., 9, 133–158, https://doi.org/10.5194/amt-9-133-2016, https://www.atmos-meas-tech.net/9/133/2016/, 2016.

Wrotny, J. E., Nedoluha, G. E., Boone, C., Stiller, G. P., and McCormack, J. P.: Total hydrogen budget of the equatorial upper stratosphere, J. Geophys. Res. Atmos., 115, https://doi.org/10.1029/2009JD012135, http://dx.doi.org/10.1029/2009JD012135, d04302, 2010.